

GEOFIK: A FAST AND RELIABLE GEOMETRIC SOLVER FOR THE IK OF THE FRANKA ARM BASED ON SCREW THEORY ENABLING MULTIPLE REDUNDANCY PARAMETERS

PREPRINT

Pablo C. Lopez-Custodio^{1*}, Yuhe Gong^{2†}, and Luis F.C. Figueredo^{2,3‡}

¹Department of Computer Science, Nottingham Trent University

²School of Computer Science, University of Nottingham

³Munich Institute of Robotics and Machine Intelligence (MIRMI), Technical University of Munich (TUM)

^{1*}pablo.lopez-custodio@ntu.ac.uk, [†]yuhe.gong@nottingham.ac.uk, [‡]figueredo@ieee.org

ABSTRACT

Modern robotics applications require an inverse kinematics (IK) solver that is fast, robust and consistent, and that provides all possible solutions. Currently, the Franka robot arm is the most widely used manipulator in robotics research. With 7 DOFs, the IK of this robot is not only complex due to its 1-DOF redundancy, but also due to the link offsets at the wrist and elbow. Due to this complexity, none of the Franka IK solvers available in the literature provide satisfactory results when used in real-world applications. Therefore, in this paper we introduce GeoFIK (Geometric Franka IK), an analytical IK solver that allows the use of different joint variables to resolve the redundancy. The approach uses screw theory to describe the entire geometry of the robot, allowing the computation of the Jacobian matrix prior to computation of joint angles. All singularities are identified and handled. As an example of how the geometric elements obtained by the IK can be exploited, a solver with the swivel angle as the free variable is provided. Several experiments are carried out to validate the speed, robustness and reliability of the GeoFIK against two state-of-the-art solvers.

1 INTRODUCTION

Inverse kinematics (IK) plays a pivotal role in robotics, bridging task-space goals with joint-space feasibility, execution, and performance. It is the core element of a wide range of tasks, from simple pick-and-place, grasping, and collision avoidance [3, 25, 24] to highly dynamic task-and-motion planning, high-DoF planning, safety [20, 17, 12] and even biomechanics [10]. Unlike forward kinematics, finding IK solutions is challenging due to the non-linearity of the equations and the branching of its solutions. While the IK of 6-DOF manipulators can have up to 16 solutions [23], the problem is more complex for redundant robots, such as 7-DOF arms, as they have infinitely many solutions organised along a continuous one-parameter family (self-motion).

Standard 7-DOF manipulators designed with spherical wrist and shoulder (without link-offsets), offer trivial kinematics which in turn allows for simple redundancy resolution. This is however not the case for the most widely used manipulator in robotics research of today [14, 11, 4, 22, 8, 9, 21], the Franka Research Robot⁴. This manipulator features an unconventional topology with non-zero joint offsets at the wrist and elbow that break the symmetry exploited by traditional solvers. Indeed, despite the excel work within the robotics community—providing modelling solutions [13, 29], and simulation environments and tools tailored exclusively for the Franka [11, 4, 22, 8]—a fundamental piece is missing: A general, fast, robust and reliable multi-parametrization analytical IK solver

In this context, this work presents the first geometry-aware IK solution for the Franka Robot based on screw theory. To address the challenges and the wide range of applications required to improve state-of-the-art methods and systems, [24, 20, 17, 12, 10, 14, 11, 4, 22, 8, 9, 21], our design choice aimed to satisfy the following conditions: The IK solver should be **(i) faster and more robust** than any other solution, also leading to more solutions than other analytical methods; **(ii) more reliable**, ensuring always finding a solution if one exists (which cannot be obtained by any sort of solver); **(iii) return feasible solutions even in extreme singular poses** where other approaches fail; **(iv) naturally return Jacobians** at no extra cost, for performance analysis; **(v) explore multiple free parameters** (beyond standard q_7), thus revealing more valid configurations than existing alternatives, including **(vi) using the swivel-angle** as a free variable, facilitating whole-body and posture analysis.

The Franka robot arm has firmly established itself as a reference system in robotics research, with a breadth of studies showing its versatility in both industrial and academic settings. Recent surveys have shown that more than 4700 papers from leading venues such as IEEE ICRA, RA-L, T-RO, IROS, CoRL, and RSS have been using the system with a majority of the work (33 %) focused on AI and ML.⁵ It is also estimated that 90 % and 100 % of the top 10 US and EU institutions in Computer Science have the system in their labs [14]. The success of the Franka arm is mostly due to its tactile and compliance capabilities as well as increased safety capabilities, including a lower effective mass at its end-effector. See the fine work of Kirschner et al. for a comparison with other systems [19]. As highlighted

⁴Franka Robotics GmbH—<https://franka.de/>

⁵Manually verified papers containing keywords *Franka robot*, *Emika*, *Panda {arm, gripper, manipulator, cobot, robot}*, or *7 DoF Panda*, 2017–23 [14].

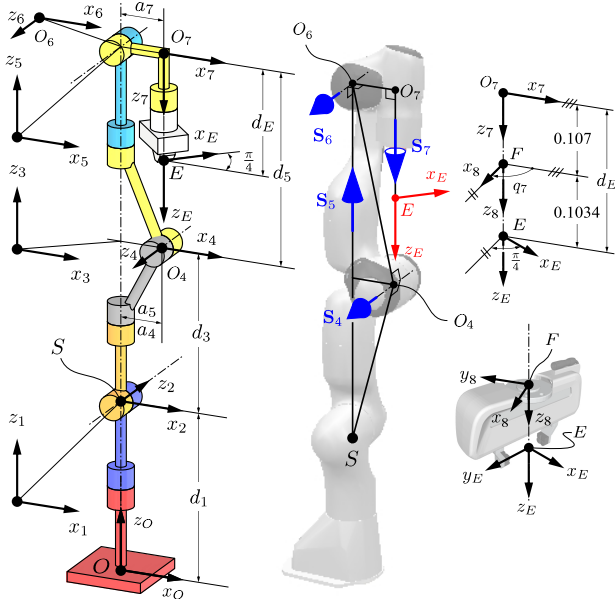


Figure 1: Home configuration of the Franka arm with $q_i = 0$, $i = 1, \dots, 7$, and detail of the end-effector frames. Note that both frames 8 and E are rigidly attached to the gripper.

in [14, 19], achieving a safer design came with a cost, an offset at the wrist (a_7) and at the elbow (a_4, a_5), which makes its IK more complex than existing systems, e.g., 7-DOF Kuka arm whose wrist and shoulder are spherical.

This complex topology (Fig. 1) reduces the effective mass—critical for safety [20, 19]—but introduces additional challenges for analytical and geometric analysis.

This challenge is reflected in the scarce number of analytical solvers for the IK of the Franka.

⁶Indeed, up to today, only four methods were capable to derive an analytical IK, [28, 30, 18, 15]. Among these results, the exceptional work by He and Liu [15] is the only complete and functional one. It is available as a C++ application [16]. Nonetheless, all the aforementioned publications limit the free parameter to the last joint, q_7 , which leads to an easier yet less robust analysis. To the best of the knowledge of the authors, no geometric solvers with other joint variables as free variable have been presented. The only available analytical solutions come from IKFast [6], which precomputes algebraic expressions of the IK to automatically generate a solver. The method is general, but this comes at the cost of lacking geometric insight, being slower than geometric methods, and instability in singularity handling. The lack of geometric insight prevents the user from extracting geometric information needed in certain applications.

⁶It is worth mentioning that an IK can always be computed numerically by means of the *differential IK* using gradient-descent, for instance, [27]. This strategy is however awfully slow, leading to hundred-to-thousand-fold slower solutions and often leading to a single solution.

1.1 Contributions

Motivated by these gaps, this paper introduces **GeoFIK** (**Geometric Franka IK**),⁷ a novel solver that systematically explores free parameters (rather than only locking q_7) while robustly handling singularities, maximizing available solutions, and offering explicit Jacobian computation at no extra cost—indeed even faster than the joint configuration.

In contrast to existing methods, including [15, 28, 6], which focus on finding individual expressions for the joint angles, our method explores the whole geometry of the robot, finding first all the screw axes. Hence, the Jacobian matrix can be returned as a byproduct. Then, the joint angles are systematically computed using the *exponential* and *logarithmic maps* of the special orthogonal group, $SO(3)$. Due to the fully geometric approach and the use of screw theory, all singularities are easily identified and handled.

In addition, as an example of the extraction of geometric information before joint angle calculation, a fast numerical IK solver that has the swivel angle as a free variable is presented. We demonstrate how it enables researchers to preserve full kinematic flexibility, guaranteeing solutions even for poses that break joint-lock-based strategies—improving robustness and reliability.

Through exhaustive quantitative analysis, we illustrate that GeoFIK outperforms existing methods in terms of reliability and robustness (leading to more solutions always finding at least one), and speed (particularly, when computing the Jacobian and joints). Furthermore, we show scenarios at singular configurations where solvers fail to converge. With real-world experiments, we also show that joint-lock-based techniques inevitably falter in discovering valid poses—even for predictably easier scenarios in the middle of the robot’s workspace—leading to potential hazard conditions, whereas our solver with swivel-angle as free variable consistently finds solutions and remains computationally efficient.

Our geometric IK solution satisfies all our design criteria from (i)-(vi) and, ultimately, can help the broader robotics community realize the full potential of the Franka Robot in both standard tasks and frontier research applications—thereby advancing the growing field of redundant manipulator control and safe human-robot collaboration.

2 PROBLEM FORMULATION AND METHOD DESCRIPTION

This section defines our IK problem, and outlines our screw-theory-based approach, its core structure and advantages, and the solution for the Franka arm.⁸

⁷The open-source C++ package for the **GeoFIK** is available in [2].

⁸Fig. 1 shows the frames and DH parameters of the Franka Robot. We use the frame E as end-effector frame for our solvers. When the gripper is connected, E matches the frame `panda_hand_tcp` in Franka Description [1]. We rename the centre of the shoulder as S . Each screw axis is collinear with the Z -axis of each frame.

Problem Definition: Given a desired pose of the end-effector frame⁹ E w.r.t. the base frame O defined by ${}^O\mathbf{r}_{E/O} \in \mathbb{R}^3$ and ${}^O\mathbf{R} \in \text{SO}(3)$ the goal is to find a set of joint-angles $q_i \in \mathbb{S}$, with $i=1, \dots, 7$ that leads to the desired pose of frame E .

Given the 1-DOF redundancy, one additional constraint must¹ be provided. This work provides multiple solutions to resolve² this redundancy including joint angles q_4, q_6 and q_7 , or defining³ a desired swivel angle.

Screw Theory-based IK Solution: Unlike traditional IK⁵ solvers that rely on purely algebraic formulations, our approach leverages geometric information from screw theory, offering an analytical and geometric perspective on the solution. The method is based on determining the screw axes of the manipulator ${}^O\mathbf{S}_i = ({}^O\hat{\mathbf{s}}_i; {}^O\mathbf{r}_i \times {}^O\hat{\mathbf{s}}_i)$, $i = 1, \dots, 7$, where ${}^O\hat{\mathbf{s}}_i$ is the direction of the axis, and ${}^O\mathbf{r}_i$ is the position of *any* point along the axis, both measured w.r.t. frame O .

By using this formulation, the **Jacobian** can be computed even without prior knowledge of joint angles as $\mathbf{J} = \text{Adj}(\mathbf{I}_3, -{}^O\mathbf{r}_{E/O})[{}^O\mathbf{S}_1, \dots, {}^O\mathbf{S}_7]$, where $\text{Adj}(\cdot, \cdot)$ is the adjoint representation of an element of $\text{SE}(3)$ defined by a pair in $\text{SO}(3) \times \mathbb{R}^3$, see Sec. 4.2 of [26].

We first exploit the spherical shoulder joint structure of the Franka, and hence we first find screw-axes ${}^O\mathbf{S}_4, {}^O\mathbf{S}_5$, and ${}^O\mathbf{S}_6$. The axis of the last joint, ${}^O\mathbf{S}_7$, is fully determined by the input, i.e., ${}^O\hat{\mathbf{s}}_7 = {}^O\hat{\mathbf{k}}_E$ and ${}^O\mathbf{r}_7 = {}^O\mathbf{r}_{E/O}$.

Once those are known, the spherical shoulder is solved as¹⁰

$$\begin{aligned} & {}^O\hat{\mathbf{s}}_3 \parallel \exp(\arctan(a_4/d_3) {}^O\hat{\mathbf{s}}_4) {}^O\mathbf{r}_{O_4/S}, \quad {}^O\hat{\mathbf{s}}_1 = (0, 0, 1)^\top, \\ & \quad {}^O\hat{\mathbf{s}}_2^{(i)} \parallel (-1)^i ({}^O\hat{\mathbf{s}}_1 \times {}^O\hat{\mathbf{s}}_3), \quad i = 1, 2, \\ & \quad {}^O\mathbf{r}_j = {}^O\mathbf{r}_{S/O} = (0, 0, d_1)^\top, \quad j = 1, 2, 3, \end{aligned}$$

Once the screw axes are known, we compute the **joint angles** by comparing how these axes rotate away from a known home configuration ($q_i=0$). Let ${}^O\hat{\mathbf{s}}_{i,0}$ be the directions of the axes at home configuration, then, from Fig. 1:

$$[{}^O\hat{\mathbf{s}}_{1,0}, \dots, {}^O\hat{\mathbf{s}}_{7,0}] = \begin{bmatrix} 0 & 0 & 0 & 0 & 0 & 0 & 0 \\ 0 & 1 & 0 & -1 & 0 & -1 & 0 \\ 1 & 0 & 1 & 0 & 1 & 0 & -1 \end{bmatrix}$$

With this information, we can compute the exponential map in $\text{SO}(3)$ to align each axis step by step. This process is shown in Algorithm 1. Note that line 4 is a simplification of $q_j \leftarrow |\log({}^O_{j+1}\mathbf{R}^\top {}^O_j\mathbf{R})|$.

Overall, our screw-based framework systematically handles the Franka's elbow/wrist offsets, provides consistent Jacobian information, and supports multiple ways to fix redundancy. These options are shown in the following sections.

In the Secs. 3, 4, 5 and 6 we present solvers that have, respectively, q_7, q_6, q_4 and swivel angle as free variable. Each

⁹The notation in [5] is used: ${}^O\mathbf{r}_{P/Q} \in \mathbb{R}^3$ is the position vector of point P with respect to point Q measured in frame O . ${}^O\mathbf{R} \in \text{SO}(3)$ is the rotation matrix defining the orientation of frame E with respect to frame O . Unit vectors wear a hat, $\hat{\mathbf{u}} \in \mathcal{S}^2$.

¹⁰We use the parallel symbol " \parallel " to avoid normalising the right-hand side when the left-hand side is a unit vector, e.i. $\hat{\mathbf{u}} \parallel \mathbf{r}$ means $\hat{\mathbf{u}} = \mathbf{r}/|\mathbf{r}|$.

Algorithm 1: Calculating the joint angles q_i from the directions of the joint axes ${}^O\hat{\mathbf{s}}_i, i = 1, \dots, 7$

Input: ${}^O\hat{\mathbf{s}}_{i,0}, {}^O\hat{\mathbf{s}}_i, i = 1, \dots, 7, {}^O\hat{\mathbf{i}}_E$

Output: q_1, \dots, q_7

$\hat{\mathbf{u}}_i \leftarrow {}^O\hat{\mathbf{s}}_{i,0}, i = 1, \dots, 7, \hat{\mathbf{u}}_8 \leftarrow (\sqrt{2}/2, \sqrt{2}/2, 0)^\top$

$\hat{\mathbf{g}}_i \leftarrow {}^O\hat{\mathbf{s}}_i, i = 1, \dots, 7, \hat{\mathbf{g}}_8 \leftarrow {}^O\hat{\mathbf{i}}_E$

for $j \leftarrow 1$ to 7 **do**

$q_j \leftarrow \text{atan2}((\hat{\mathbf{u}}_{j+1} \times \hat{\mathbf{g}}_{j+1}) \cdot \hat{\mathbf{u}}_j, \hat{\mathbf{u}}_{j+1} \cdot \hat{\mathbf{g}}_{j+1})$
 $[\hat{\mathbf{u}}_{j+1}, \dots, \hat{\mathbf{u}}_8] \leftarrow \exp(q_j \hat{\mathbf{u}}_j) [\hat{\mathbf{u}}_{j+1}, \dots, \hat{\mathbf{u}}_8]$

solver has as input the value of the free variable, and ${}^O\hat{\mathbf{i}}_E, {}^O\hat{\mathbf{s}}_7 = {}^O\hat{\mathbf{k}}_E$, and ${}^O\mathbf{r}_{O_7/O} = {}^O\mathbf{r}_{E/O} - d_E {}^O\hat{\mathbf{k}}_E$ (and ${}^O\mathbf{r}_{O_7/S}$). The goal is to find ${}^O\mathbf{S}_4, {}^O\mathbf{S}_5$ and ${}^O\mathbf{S}_6$.

3 SOLUTION LOCKING JOINT 7

It can be seen that ${}^O\hat{\mathbf{s}}_6 = \exp((\frac{3}{4}\pi - q_7) {}^O\hat{\mathbf{s}}_7) {}^O\hat{\mathbf{i}}_E$ and ${}^O\mathbf{r}_6 = {}^O\mathbf{r}_{O_6/O} = {}^O\mathbf{r}_{O_7/O} - a_7 {}^O\hat{\mathbf{s}}_6 \times {}^O\hat{\mathbf{s}}_7$.

Consider ${}^O\mathbf{r}_{O_6/S} = {}^O\mathbf{r}_{O_6/S} - {}^O\mathbf{r}_{S/O}$ and let $l := |{}^O\mathbf{r}_{O_6/S}|$, $b_1 := \sqrt{d_3^2 + a_4^2}$, $b_2 := \sqrt{d_5^2 + a_5^2}$, $\rho_1 := \arctan(a_4/d_3)$ and $\rho_2 := \arctan(a_5/d_5)$ in Fig. 2, then:

$$\alpha_2^{(1)} = \rho_2 + \beta_2, \quad \alpha_2^{(2)} = \rho_2 - \beta_2, \quad (1)$$

$$\text{with } \beta_2 := \arccos((b_1^2 - b_2^2 - l^2)/(-2b_2l)).$$

These two solutions correspond to the elbow-up and elbow-down assemblies of triangle SO_4O_6 . However, as noted in [15], due to link interference, solution 2 only happens when SO_4O_6 is almost flat and $d_3 + d_5 < l < b_1 + b_2$, Fig. 8 shows one of such scenarios.

Define a frame C with ${}^O\hat{\mathbf{k}}_C \parallel {}^O\mathbf{r}_{S/O_6}$ and ${}^O\hat{\mathbf{i}}_C \parallel {}^O\hat{\mathbf{k}}_C \times {}^O\hat{\mathbf{s}}_6$. This allows us to easily write ${}^C\hat{\mathbf{s}}_5 = -(\sin \alpha_2 \cos \gamma, \sin \alpha_2 \sin \gamma, \cos \alpha_2)^\top$, where, if ${}^C\hat{\mathbf{s}}_6 = {}^C\mathbf{R} {}^O\hat{\mathbf{s}}_6 = (0, s_{6,y}, s_{6,z})$, imposing the constraint ${}^C\hat{\mathbf{s}}_5 \cdot {}^C\hat{\mathbf{s}}_6 = 0$ results in:

$$\gamma^{(1)} = \arcsin(A_\gamma), \quad \gamma^{(2)} = \pi - \arcsin(A_\gamma),$$

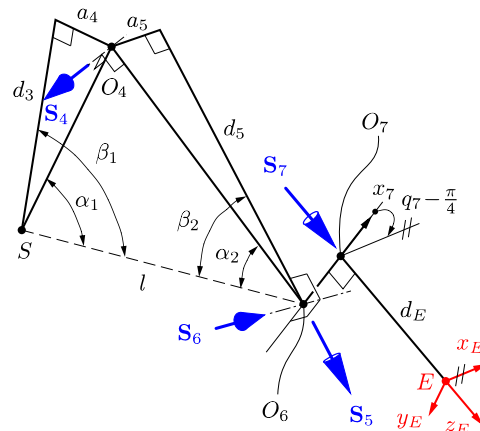
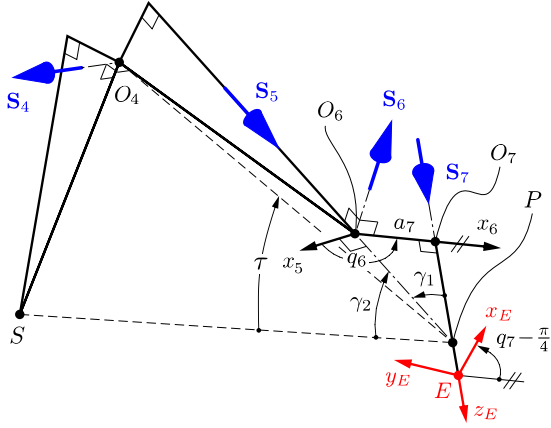
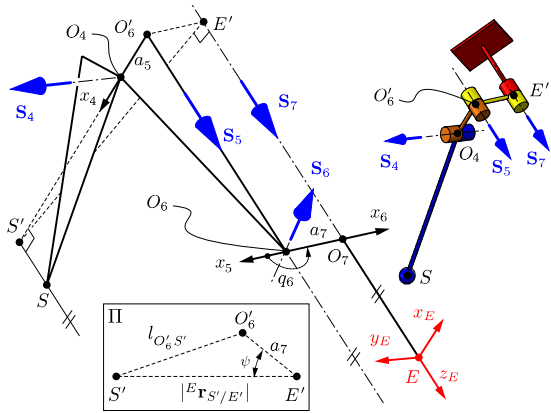


Figure 2: Franka Robot Geometry for the IK solution fixing q_7 .

Figure 3: Geometry of the Franka for the IK fixing $q_6 \notin \{0, \pi\}$.Figure 4: Geometry of the Franka for the IK fixing $q_6 \in \{0, \pi\}$.

where, $A_\gamma := -(s_{6,z}/s_{6,y}) \cot \alpha_2$. If $A_\gamma > 1$, the kinematic chain cannot be assembled, and if $A_\gamma = 1$ the two solutions for γ are repeated. Finally, ${}^O\hat{\mathbf{s}}_5 = {}^O\mathbf{R}^C \hat{\mathbf{s}}_5$ and ${}^O\mathbf{r}_5 = {}^O\mathbf{r}_6$. The remaining parameters are easily found as follows:

$${}^O\hat{\mathbf{s}}_4 \parallel {}^O\hat{\mathbf{s}}_5 \times {}^O\mathbf{r}_6, \quad {}^O\mathbf{r}_4 = {}^O\mathbf{r}_6 - d_5 {}^O\hat{\mathbf{s}}_5 + a_5 {}^O\hat{\mathbf{s}}_5 \times {}^O\hat{\mathbf{s}}_4.$$

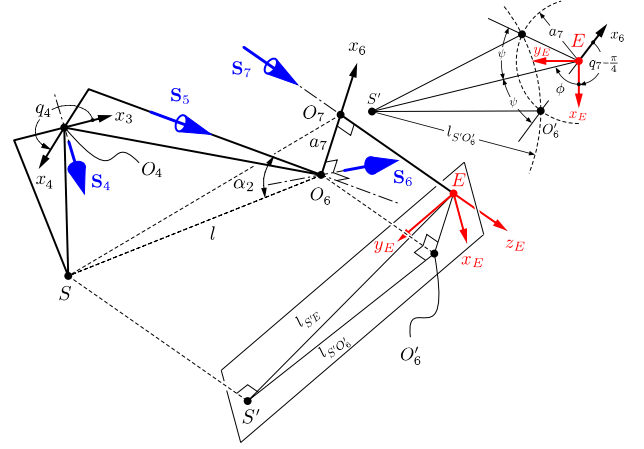
Since α_2 , γ and ${}^O\hat{\mathbf{s}}_2$ can have up to two solutions each, the maximum number of solutions is $2^3 = 8$.

4 SOLUTION LOCKING JOINT 6

Define $\gamma_1 := \pi - q_6$ as the angle between \mathbf{S}_5 and \mathbf{S}_7 , and let P be their intersection point as shown in Fig. 3. The following two cases are analysed separately.

\mathbf{S}_5 and \mathbf{S}_7 are not parallel: It can be seen that ${}^O\mathbf{r}_{P/S} = {}^O\mathbf{r}_{O_7/S} + (a_7/\tan \gamma_1) {}^O\hat{\mathbf{k}}_E$. Let γ_2 be the angle from $\mathbf{r}_{S/P}$ to $-\mathbf{S}_5$ measured about $-\hat{\mathbf{s}}_4$ as shown in Fig. 3. The goal is to first find γ_2 using the polygon SO_4O_6P and then use the result to find $\hat{\mathbf{s}}_5$.

Let l_C be the projection of \mathbf{r}_{P/O_6} on \mathbf{S}_5 , so $l_C = a_7/\sin \gamma_1$. The angle τ , defined as $\angle SPO_4$ can be easily found by solving first the triangle PO_6O_4 followed by triangle SPO_4 . It can be

Figure 5: Geometry of the Franka for the IK solution fixing q_4 .

seen that

$$\gamma_2^{(1)} = \begin{cases} \tau + \arctan(a_5/(d_5 + l_C)) + \pi & \text{if } l_C < -d_5, \\ \tau + \arctan(a_5/(d_5 + l_C)) & \text{otherwise} \end{cases}$$

The extreme case when SPO_4 is almost flat, i.e. $d_3 + d_5 + l_C < |{}^O\mathbf{r}_{S/P}| < b_1 + (a_5^2 + (l_C + d_5)^2)^{1/2}$, provides a second solution $\gamma_2^{(2)}$ in which τ appears with negative sign.

Now we can write an equation to constrain the angle between $\mathbf{r}_{S/P}$ and \mathbf{S}_5 to γ_2 . In frame E it is easy to write ${}^E\hat{\mathbf{s}}_5 = (-\sin \gamma_1 \cos u, -\sin \gamma_1 \sin u, \cos \gamma_1)^\top$, where $u := 5\pi/4 - q_7$. Then, the following equation in u is to be solved:

$$-{}^E\hat{\mathbf{s}}_5 \cdot {}^E\mathbf{r}_{S/P} = {}^E\hat{\mathbf{s}}_5 \cdot ({}^O\mathbf{R})^\top {}^O\mathbf{r}_{P/S} = |{}^O\mathbf{r}_{P/S}| \cos \gamma_2$$

which has the two solutions $u^{(1)} = u_1 - u_2$ and $u^{(2)} = \pi - u_1 - u_2$, where, if ${}^E\mathbf{r}_{S/P} = (C_1, C_2, C_3)^\top$:

$$u_1 := \arcsin \left(\frac{|{}^O\mathbf{r}_{P/S}| \cos \gamma_2 + C_3 \cos \gamma_1}{|\sin \gamma_1| \sqrt{C_1^2 + C_2^2}} \right),$$

$$u_2 := \text{atan2}(C_1 \sin \gamma_1, C_2 \sin \gamma_1)$$

With ${}^O\mathbf{r}_{P/O} = {}^O\mathbf{r}_{P/S} + {}^O\mathbf{r}_{S/O}$, the remaining parameters are found easily:

$${}^O\mathbf{r}_5 = {}^O\mathbf{r}_6 = {}^O\mathbf{r}_{O_6/O} = {}^O\mathbf{r}_{P/O} - l_C {}^O\hat{\mathbf{s}}_5,$$

$${}^O\hat{\mathbf{s}}_6 \parallel {}^O\hat{\mathbf{k}}_E \times ({}^O\mathbf{r}_{O_7/O} - {}^O\mathbf{r}_{O_6/O}), \quad {}^O\hat{\mathbf{s}}_4 \parallel {}^O\hat{\mathbf{s}}_5 \times {}^O\mathbf{r}_{P/S},$$

$${}^O\mathbf{r}_4 = {}^O\mathbf{r}_{O_4/O} = {}^O\mathbf{r}_{P/O} - (d_5 + l_C) {}^O\hat{\mathbf{s}}_5 + a_5 {}^O\hat{\mathbf{s}}_5 \times {}^O\hat{\mathbf{s}}_4$$

Since γ_2 , u and ${}^O\hat{\mathbf{s}}_2$ have up to two solutions, the maximum number of solutions is $(2)^3 = 8$.

\mathbf{S}_5 and \mathbf{S}_7 are parallel: Since $q_6 \in \{0, \pi\}$, we define $\sigma = \cos q_6 \in \{1, -1\}$. Consider the plane Π which is perpendicular to \mathbf{S}_5 and \mathbf{S}_7 and contains \mathbf{S}_4 , see Fig. 4. Let E' , O'_6 and S' be the respective projections of E , O_6 and S onto Π . Note that ${}^E\mathbf{r}_{E'/E} = (0, 0, -d_E + \sigma d_5)^\top$. Since E' is known, the problem is reduced to solving the equivalent kinematic chain shown in Fig. 4 by working on plane Π and in frame E .

It can be seen that ${}^E\mathbf{r}_{S'/E'} = {}^E\mathbf{r}_{S/E'} - ({}^E\mathbf{r}_{S/E'} \cdot {}^E\hat{\mathbf{k}}_E) {}^E\hat{\mathbf{k}}_E$, where ${}^E\mathbf{r}_{S/E'} = {}^E\mathbf{r}_{S/E} - {}^E\mathbf{r}_{E'/E}$. Due to the two possible

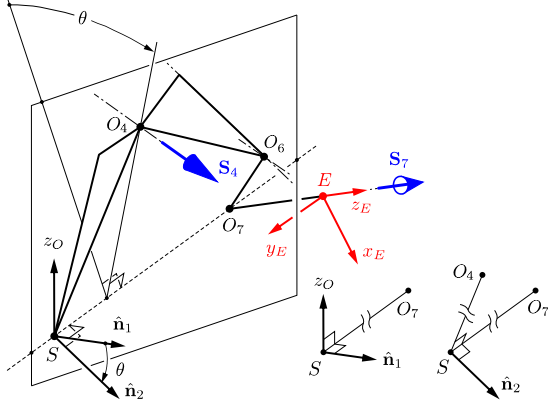


Figure 6: Geometry of the Franka arm for the IK solution fixing the swivel angle θ .

ways of reaching S from Π , the distance from O'_6 to S' along x_4 is $l_{O'_6 S'}^{(i)} = a_5 + (-1)^i (d_3^2 + a_4^2 - ({}^E \mathbf{r}_{S/E'} \cdot {}^E \hat{\mathbf{k}}_E)^2)^{1/2}$, $i = 1, 2$. This leads to two solutions for ψ , the angle $\angle S'E'O'_6$:

$$\psi^{(i)} = \arccos \left[\frac{(l_{O'_6 S'}^{(i)})^2 - a_7^2 - |{}^E \mathbf{r}_{S'/E'}|^2}{-2a_7 |{}^E \mathbf{r}_{S'/E'}|} \right], \quad i = 1, 2.$$

Similarly, due to the two different ways of assembling the triangle $S'E'O'_6$, two solutions for the position of O'_6 appear for each solution of ψ :

$${}^E \mathbf{r}_{O'_6/E'} = a_7 \exp((-1)^i \psi {}^E \hat{\mathbf{k}}_E) {}^E \mathbf{r}_{S'/E'} / |{}^E \mathbf{r}_{S'/E'}|, \quad i = 1, 2.$$

It follows that ${}^E \mathbf{r}_6 = {}^E \mathbf{r}_{E'/E} + {}^E \mathbf{r}_{O'_6/E'} - \sigma d_5 {}^E \hat{\mathbf{k}}_E$ and ${}^E \hat{\mathbf{s}}_6 \parallel {}^E \mathbf{r}_{O'_6/E'} \times {}^E \hat{\mathbf{k}}_E$. For ${}^E \mathbf{S}_5$, it can be seen that ${}^E \hat{\mathbf{s}}_5 = -\sigma {}^E \hat{\mathbf{k}}_E$ and ${}^E \mathbf{r}_5 = {}^E \mathbf{r}_6$. To find ${}^E \mathbf{S}_4$, consider ${}^E \hat{\mathbf{i}}_4 \parallel \text{sign}(l_{O'_6 S'}) ({}^E \mathbf{r}_{S'/E'} - {}^E \mathbf{r}_{O'_6/E'})$, then ${}^E \mathbf{r}_4 = {}^E \mathbf{r}_{E'/E} + {}^E \mathbf{r}_{O'_6/E'} + a_5 {}^E \hat{\mathbf{i}}_4$, and ${}^E \hat{\mathbf{s}}_4 = {}^E \hat{\mathbf{i}}_4 \times {}^E \hat{\mathbf{s}}_5$. All the screw axes are then transformed back to frame O .

Since ψ , ${}^E \mathbf{r}_{O'_6/E'}$ and ${}^O \hat{\mathbf{s}}_2$ can have up to two solutions each, the maximum number of solutions is $2^3 = 8$.

5 SOLUTION LOCKING JOINT 4

Since in this case q_4 is given, the triangle SO_4O_6 can be easily solved to obtain $l := |\mathbf{r}_{S/O_6}|$ and α_2 , see Fig. 5. We can then locate O_6 on a sphere of radius l and centre at S . From the pose of frame E , we can also constrain O_6 to a known circle of radius a_7 and centre at O_7 . Hence, the problem is solved by finding the intersection of this circle with the sphere. This is reduced to the intersection of two circles on the $X_E Y_E$ -plane.

As shown in Fig. 5, let S' and O'_6 be the respective projections of points S and O_6 onto the $X_E Y_E$ -plane, then define $l_{S'O'_6} := |\mathbf{r}_{S'/O'_6}| = (l^2 - ({}^E \mathbf{r}_{O_7/S} \cdot {}^E \hat{\mathbf{k}}_E)^2)^{1/2}$ and $l_{S'E'} := |\mathbf{r}_{S'/E'}| = (({}^E \mathbf{r}_{O_7/S} \cdot {}^E \hat{\mathbf{i}}_E)^2 + ({}^E \mathbf{r}_{O_7/S} \cdot {}^E \hat{\mathbf{j}}_E)^2)^{1/2}$.

To find O'_6 , consider ϕ , the angle from x_E to $\mathbf{r}_{S'/E'}$ about z_E , and ψ , the angle $\angle S'E'O'_6$, as shown in Fig. 5. It can be seen that $\phi = \text{atan2}({}^E \mathbf{r}_{S/O_7} \cdot {}^E \hat{\mathbf{j}}_E, {}^E \mathbf{r}_{S/O_7} \cdot {}^E \hat{\mathbf{i}}_E)$ and

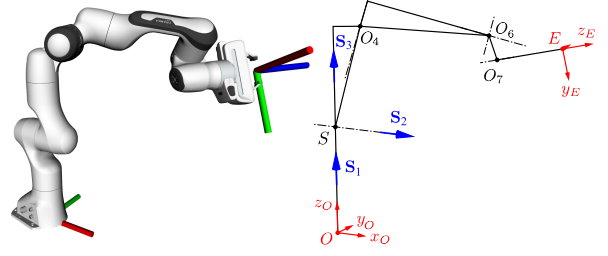


Figure 7: Configuration in a type-1 singularity.

$\psi = \arccos((l_{S'E'}^2 + a_7^2 - l_{S'O'_6}^2)/(2a_7 l_{S'E'}))$, leading to the two solutions $q_7^{(i)} = (-1)^i \psi - \phi - 3\pi/4$, $i = 1, 2$.

With O'_6 in hand, it is easy to find ${}^O \mathbf{S}_6$ with ${}^O \hat{\mathbf{s}}_6 = {}^O \mathbf{R} \exp((-q_7 + 3\pi/4) {}^E \hat{\mathbf{k}}_E) {}^E \hat{\mathbf{i}}_E$ and ${}^O \mathbf{r}_{O_6/O} = {}^E \mathbf{R} {}^E \mathbf{r}_{O_6/O_7} + {}^O \mathbf{r}_{O_7/O}$, where ${}^E \mathbf{r}_{O_6/O_7} = -a_7 \exp((-q_7 + \pi/4) {}^E \hat{\mathbf{k}}_E) {}^E \hat{\mathbf{i}}_E$.

Since q_7 , ${}^O \mathbf{S}_6$ and α_2 are known now, we can proceed as we did in Sec. 3, where q_7 was a free parameter. Following the same procedure, we find two solutions of ${}^O \hat{\mathbf{s}}_5$ per each value of q_7 .

Since q_7 , ${}^O \hat{\mathbf{s}}_5$ and ${}^O \hat{\mathbf{s}}_2$ can have up to two solutions each, the total number of solutions is $2^3 = 8$.

6 SOLUTION FOR SWIVEL ANGLE

Due to the lack of a spherical wrist, the swivel angle θ can be defined using either O_6 or O_7 as “wrist centre”. Let this be O_7 , like in [31]. Then the swivel angle is defined between the plane containing z_O and O_7 , and the plane containing O_4 , S and O_7 as shown in Fig. 6. Hence, if:

$${}^O \hat{\mathbf{n}}_1 \parallel {}^O \mathbf{r}_{O_7/S} \times {}^O \hat{\mathbf{k}}_O \quad \text{and} \quad {}^O \hat{\mathbf{n}}_2 \parallel \sigma {}^O \mathbf{r}_{O_7/S} \times {}^O \mathbf{r}_{O_4/S}$$

with $\sigma = \text{sign}({}^O \mathbf{r}_{O_7/S} \times {}^O \mathbf{r}_{O_4/S} \cdot {}^O \hat{\mathbf{s}}_4)$

then θ is the angle from ${}^O \hat{\mathbf{n}}_1$ to ${}^O \hat{\mathbf{n}}_2$ measured about ${}^O \mathbf{r}_{O_7/S}$. Clearly, θ is not defined if $\mathbf{r}_{O_7/S}$ is parallel to z_O . This is the unavoidable singularity of any swivel angle definition [7].

In order to find all the solutions that have the desired value of θ , we discretise the range of q_7 , calculate θ for each point, pick the ones that are close enough to the desired value, and finally we interpolate to find the optimal values of q_7 . q_7 is used as free variable since, by doing so, the first singularity discussed in Sec. 7 is avoided.

We do not need to solve the entire IK with q_7 as input, we only obtain the strictly necessary geometric elements that allow us to calculate θ . That means proceeding as done in Sec. 3 until ${}^O \mathbf{r}_7$, ${}^O \mathbf{r}_6$ and ${}^O \hat{\mathbf{s}}_4$ are found. To speed up the process, we ignore the elbow-down solution with $\alpha_2^{(2)}$ in Eq. (1), which appears in the unlikely cases where $d_3 + d_5 < l < b_1 + b_2$.

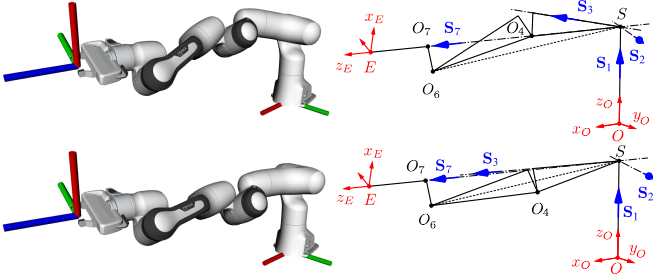


Figure 8: Elbow-up and elbow-down solutions in a type-2 singularity. Note that these are *not* work-space boundary singularities as the arm is not fully stretched.

7 SINGULARITY ANALYSIS

Let \mathcal{S} be the screw system spanned by the screw axes. Given the topology and joint limits of the Franka arm, the dimension of \mathcal{S} can only drop in the following two scenarios:

Type 1: \mathbf{S}_1 is collinear with \mathbf{S}_3 : This singularity is well-reported in [15, 28]. In this case $\dim(\text{span}(\{\mathbf{S}_1, \mathbf{S}_2, \mathbf{S}_3\})) = 2$ causing \mathcal{S} have dimension 6. However, if q_1 is provided, \mathbf{S}_1 is removed from the screw system, and the remaining 6 screws are linearly-independent. The user can provide an emergency value of q_1 to be used in case this situation occurs. In this singularity, the spherical shoulder can experience self-motion, with the links connected by \mathbf{S}_2 spinning about $\mathbf{S}_1 = \mathbf{S}_3$ without affecting the rest of the robot. Fig. 7 shows an example of type-1 singularity.

Type 2: \mathbf{S}_7 intersects the spherical shoulder at O : In this case, $\text{span}(\{\mathbf{S}_1, \mathbf{S}_2, \mathbf{S}_3\}) = \text{span}(\{\mathbf{S}_1, \mathbf{S}_2, \mathbf{S}_3, \mathbf{S}_7\})$, and the dimension of \mathcal{S} drops to 6. However, if q_7 is provided, \mathbf{S}_7 is no longer part of the system, and the remaining 6 axes are linearly independent. Therefore, the solver with q_7 as free variable (Sec. 3) is free of this singularity. For the other solvers, if it is found that $S \in \mathbf{S}_7$, the solver with q_7 as free variable is called with an emergency value of q_7 provided by the user. However, it is easy to prove geometrically that, in this type of singularity, there are only two or four possible ways to assembly the polygon $SO_4O_6O_7$. Hence, q_6 and q_4 are no longer free choices and the solvers must ignore their requested values. The robot experiences self-motion with the polygon $SO_4O_6O_7$ spinning around \mathbf{S}_7 without affecting q_4, q_5 and q_6 . Fig. 8 shows an example of type-2 singularity.

8 COMPARISON WITH BASELINE SOLVERS

This section presents an analytical comparison against the state-of-the-art solvers from He and Liu [15], which we will refer to as HeLiu, and IKFast [6]. When locking q_7 , we evaluate against both methods, while for other free variables, only IKFast is available, as HeLiu only provides a q_7 -solver.

8.1 Number of solutions attempted

As discussed in Sections 3-5, each case of GeoFIK solver attempts 8 solutions which constitute all geometrically valid solutions. By contrast, HeLiu attempts only 4 solutions, explicitly

Table 1: Solver Comparison for Singular Configurations (angles are in degrees, violation of joint limits are in red).

Case 1 (Type-1 singularity, solvers with q_7 as free variable)								
sol	q_1	q_2	q_3	q_4	q_5	q_6	q_7	
GeoFIK (ours)	1	-30.06	86.09	123.97	-106.86	48.58	nan	-21.32
	2	149.94	-86.09	-56.03	-106.86	48.58	nan	-21.32
	3	-90	0	115.96	-106.86	131.42	150.52	-21.32
	4	90	0	-64.04	-106.86	131.42	150.52	-21.32
HeLiu	1	90	0	-64.04	-106.86	131.42	150.52	-21.32
	2	90	0	-64.04	-106.86	131.42	150.52	-21.32
	3	-30.06	86.09	123.97	nan	nan	nan	nan
	4	149.94	-86.09	-56.03	nan	nan	nan	nan
IKFast	1	-30.06	86.09	123.97	-106.86	48.58	-137.3	-21.32
	2	149.94	-86.09	-56.03	-106.86	48.58	-137.3	-21.32
Case 2 (Type-2 singularity, solvers with q_6 as free variable)								
sol	q_1	q_2	q_3	q_4	q_5	q_6	q_7	
GeoFIK (ours)	1	-18.99	78.13	28.75	-39.33	0	204.90	0
	2	161.01	-78.13	-151.25	-39.33	0	204.90	0
	3	2.37	nan	-148.49	-39.33	nan	169.24	0
	4	nan	nan	31.51	-39.33	nan	169.24	0
	5	-12.43	90.22	28.08	-14.19	0	193.44	0
	6	nan	-90.22	-151.92	-14.19	0	193.44	0
	7	-4.97	nan	-151	-14.19	nan	180.65	0
	8	nan	nan	29	-14.19	nan	180.65	0
IKFast	no solution							

omitting a secondary elbow-down (solution 2 in Eq. (1)), as acknowledged in [15]. Due to its general algebraic approach, IKFast attempts the 16 solutions that the system of equations can have. However, since only 8 solutions are geometrically possible, the other 8 must be complex or repeated. Among those, IKFast will return elbow-down solutions with link interference which have to be discarded by subsequent joint-limits checks.

8.2 Handling of singularities

We examine the behaviour of the solvers in the two types of singularities described in Sec. 7.

Type-1 singularities: Consider the following IK problem that leads to a type-1 singularity:

$${}^O_E\mathbf{R} = \begin{pmatrix} 0.6688331 & 0.31705344 & 0.672413 \\ -0.6398146 & -0.21507724 & 0.7378205 \\ 0.3785493 & -0.92369843 & 0.0590046 \end{pmatrix},$$

$${}^O\mathbf{r}_{E/O} = (0.61674948, 0.32278029, 0.56790512)^\top,$$

$$q_7 = -21.32455095^\circ.$$

The problem is sent to the solvers with q_7 as a free parameter. The results are shown as Case 1 in Table 1.

In GeoFIK, the user can provide a value of q_1 to resolve the redundancy. The default value is $\pi/2$. Solutions for the two ways of assembling the spherical shoulder are still returned with $\pm q_1$. One such solution is shown in Fig. 7. Other two solutions that are not singular are returned, however, in those q_6 violates joint limits. In HeLiu, the user provides a vector of joint angles from which it takes q_1 and uses it to resolve the redundancy induced by the singularity. Then, it returns two repeated solutions with q_1 , rather than two different ones with $\pm q_1$ —which can lead to discontinuity in the real-world applications—and the other two regular solutions that violate joint limits. IKFast fails entirely under this singular configuration and only returns the two regular configurations that violate joint limits.

Type-2 singularities: Consider the following IK problem that leads to a type-2 singularity:

$${}^O_E\mathbf{R} = \begin{pmatrix} 0.0746454 & -0.1964604 & 0.9776662 \\ 0.281646 & -0.93633263 & -0.2096583 \\ 0.9566105 & 0.2910058 & -0.0145606 \end{pmatrix},$$

$${}^O\mathbf{r}_{E/O} = (0.89948341, -0.1928922, 0.31960372)^\top,$$

$$q_6 = 193.48937052^\circ.$$

The problem is sent to the solvers with q_6 as a free parameter. The results are shown as Case 2 in Table 1.

In type-2 singularities, q_6 stops being a free variable as there are only two values of q_6 that satisfy the IK problem. In this particular case, we lock q_6 to one of the valid values $q_6 = 193.489^\circ$.

GeoFIK is able to automatically detect that q_6 can no longer be freely chosen and transfers the problem to the solver with q_7 as a free variable. 8 solutions are found, indicating that triangle SO_4O_6 is almost flat, allowing elbow-up and elbow-down solutions as shown in Fig. 8. Among those, two solutions are within the locked value for q_6 .

IKFast fails to generate any solution even though the requested value of q_6 allows to assembly the robot with the pose requested. It is worth highlighting that this behaviour is inconsistent as IKFast is able to find solutions to some type-2 singularities (yet, it is highly sensitive to numerical precision to work). This is not an issue with GeoFIK, since once it detects the singularity, it no longer requires the value of q_6 . Hence, it returns consistently valid solutions.

9 QUANTITATIVE ANALYSIS

To quantitatively evaluate the performance of our IK framework under controlled conditions, we compared it against [15] (HeLiu) and [28] on the same hardware¹¹ We generated 2000 random valid joint configurations to produce EE poses, which in turn were sent as input to the solvers.

In terms of performance, we evaluated all the solvers against five parameters. The results are shown in Table 2.

(i) Computational time for a single call—including sole *joint-solutions*, sole *Jacobians*, and the time for finding the set of feasible *joint and Jacobian solutions*.

When q_7 was locked our solver matched HeLiu’s computation time and significantly outperformed IKFast. This was the only experiment where we used aggressive optimization methods for *all solvers*,¹²All following experiments were performed with O3 and release flags alone (for all solvers). When comparing the Jacobian computation time, GeoFIK outperformed all other solvers. This is mostly due to our screw-axes-based design that returns the Jacobian as a byproduct of the IK. It is worth mentioning, GeoFIK outputs Jacobians even faster than the joint-

configurations. When using q_6 and q_4 as free-variables, GeoFIK also outperformed IKFast in all cases.

(ii) Max. Number of Solutions provided; **(iii) Max. Number of Non-Zero Solutions**, that is, *successful calls*; **(iv) EE Error – Position and Rotation**; and **(v) Highest manipulability**, in terms of the ellipsoid volume, determinant-based as in [3].

Our approach provided more valid solutions than HeLiu. IKFast provided slightly more, but those include unfeasible elbow configurations and out-of-range solutions. This can result in issues in real-robot experiments—as shown in Section 10.

At the same time, our approach yielded more valid solutions than HeLiu, maintaining lower end-effector position and orientation errors. Although IKFast appeared to generate the smallest error in some tests, many of its solutions disregarded joint constraints and were not physically realizable. The same result is also reflected within the manipulability analysis.

The reliability of our method is further reflected by the *Num. of Non-Zero Solution* which depicts the number of successful calls—at least, one valid solution. Here, it is interesting to show that using Swivel-angle as a free-variable ensures at least one solution is always returned. This 100% performance is illustrated in real-world experiments, as shown in Fig. 9.

10 REAL-WORLD EXPERIMENT

We evaluated our GeoFIK approach on a real Franka Robot to investigate (i) feasibility and joint-space tracking of a desired task-space trajectory (herein obtained through vector fields) within the robot’s central workspace, and (ii) whole-body tasks that require both the end-effector pose and the manipulability ellipsoid to match a human-demonstrated reference (i.e., sweeping and pushing).

Feasibility and Trajectory Tracking: This first scenario tested each solver’s ability to compute real-time IKs and maintain a continuous joint-space trajectory over a basic trajectory in the central region of the workspace, a domain expected to be straightforward. Despite this assumption, the IK solver by HeLiu failed after approximately 10 s, providing no valid solutions and forcing the robot to halt. Our GeoFIK solver, when using q_7 as the free parameter, also reached a point where it could not find a solution. Both failures led to abrupt reconfiguration once a valid solution was found again, causing excessive motion and potential spillage of the cup content (Fig. 9 top-images with a red border).

Allowing the standard q_7 -locking solvers to “sample” a small range $\pm 10^\circ$ around the current q_7 mitigated total failure, but induced frequent chattering in joint angles (Fig. 10). Meanwhile, IKFast remained unable to find even a valid initial solution, all valid IKs demand an instantaneous flip of the base joints, generating torque reflexes and halting progress altogether, as shown in Fig. 12(a).

In contrast, the swivel-angle-based GeoFIK solution never lost feasibility (as expected from Table 2) and preserved a smooth trajectory as shown in Fig 9 even without sampling.

Whole-Body (Manipulability) Tracking: The second set of experiments required each solver to produce both joint angles

¹¹The computer used in this work: AMD Ryzen 7 5800H, 32GB DDR4-3200 running Ubuntu 20.04 with gcc/g++ 9.4 and clang 10.0.

¹²Opt. flags: -DCMAKE_BUILD_TYPE=Release -DCMAKE_CXX_FLAGS="-O3 -march=native -mtune=native -ffast-math -funroll-loops", -DCMAKE_C_COMPILER=clang, -DCMAKE_CXX_COMPILER=clang++.

Table 2: IK Solver Quantitative Comparison in terms of computation time, number of solutions, non-zero solutions, errors.

Min/Median/Max Mean \pm Std	Locking q_7 (optimized)			Locking q_6		Locking q_4		Locking S. Angle
	GeoFIK	Helium	IKFast	GeoFIK	IKFast	GeoFIK	IKFast	GeoFIK
Joint Comp. Time (μ s)	0.9/2.9/35 3.1 \pm 1.7	0.9/2.8/37 3.1 \pm 1.4	0.9/5.2/33 5.8 \pm 3.1	0.9/3.8/32 4.1 \pm 1.8	29/41/243 43 \pm 12	0.9/6.6/50 6.4 \pm 2.4	0.9/4.8/86 5.7 \pm 3.2	26/95/287 89 \pm 387
Jacobian Comp. Time (μ s)	0.8/1.4/38 1.6 \pm 1.2	— —	— —	0.9/2.4/72 2.3 \pm 2.4	— —	0.9/2.4/45 2.6 \pm 1.9	— —	27/95/274 91 \pm 388
Jacobian + Joint Comp. Time (μ s)	0.9/3.8/22 4.5 \pm 2.1	3.4/5.7/43 5.8 \pm 1.5	0.9/11/59 14 \pm 5.5	0.9/5.2/92 5.5 \pm 5.2	33/49/171 51 \pm 13	0.9/8.5/56 8.6 \pm 3.6	1.4/13/85 15 \pm 5.5	26/99/258 92 \pm 396
Num. of Solution	0/4/8 4.6 \pm 1.5	0/2/4 2.6 \pm 1.0	0/4/10 5.5 \pm 2.0	0/2/8 2.2 \pm 1.5	0/4/12 5.9 \pm 2.3	0/4/8 3.6 \pm 2.3	0/8/16 8.8 \pm 1.8	1/8/4 3.1 \pm 1.2
Num of Non-Zero Solution	1997	1238	1998	1781	1998	1849	1997	2000
EE. Error Pos.	$\cdot /1e^{-7}/0.02$ 5e $^{-5}$ \pm 8e $^{-4}$	$\cdot /9e^{-8}/0.04$ 1e $^{-4}$ \pm 2e $^{-3}$	$\cdot /1e^{-7}/0.02$ 5e $^{-5}$ \pm 7e $^{-4}$	$\cdot /3e^{-7}/0.12$ 2e $^{-3}$ \pm 7e $^{-3}$	$\cdot /4e^{-7}/0.12$ 6e $^{-4}$ \pm 4e $^{-3}$	$\cdot /2e^{-7}/0.02$ 1e $^{-4}$ \pm 8e $^{-4}$	$\cdot /3e^{-7}/0.02$ 5e $^{-5}$ \pm 5e $^{-4}$	$\cdot /1e^{-7}/0.02$ 6e $^{-5}$ \pm 7e $^{-4}$
EE. Error Rot.	$\cdot /3e^{-7}/0.03$ 9e $^{-5}$ \pm 1e $^{-3}$	$\cdot /1e^{-7}/0.04$ 2e $^{-4}$ \pm 2e $^{-3}$	$\cdot /3e^{-7}/0.03$ 7e $^{-5}$ \pm 1e $^{-3}$	$\cdot /2e^{-7}/0.03$ 5e $^{-5}$ \pm 9e $^{-4}$	$\cdot /3e^{-7}/0.03$ 2e $^{-5}$ \pm 6e $^{-4}$	$\cdot /2e^{-7}/0.03$ 4e $^{-5}$ \pm 8e $^{-4}$	$\cdot /3e^{-7}/0.03$ 3e $^{-7}$ \pm 5e $^{-4}$	$\cdot /3e^{-7}/0.03$ 1e $^{-4}$ \pm 1e $^{-3}$
Max. Manip. (e^{-3})	3.3 \pm 3.6	2.8 \pm 3.5	3.4 \pm 3.7	2.2 \pm 3.4	3.0 \pm 3.6	3.1 \pm 3.8	3.9 \pm 4.1	2.3 \pm 3.0

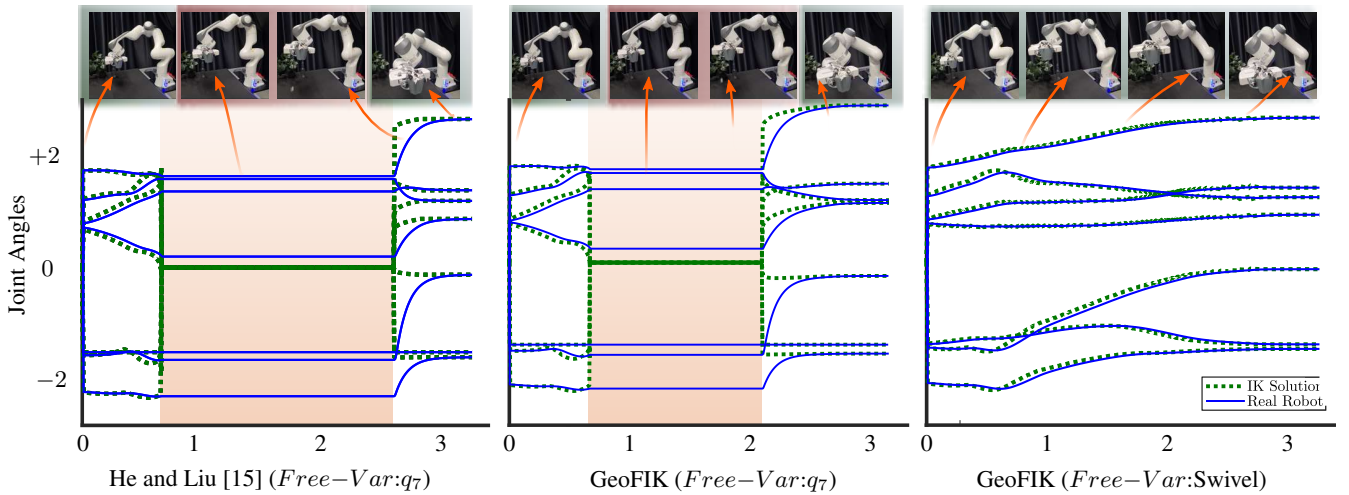


Figure 9: Trajectory tracking using IK solvers: The obtained joints (dashed-green lines) compared to the real-robot (blue lines). HeLiu and GeoFIK (with q_7 as a free-var) both fail to find a feasible solution around 10 s. (shaded area) and the robot stops (real-robot on the top strip) only to continue with an aggressive motion at the end of the trajectory. GeoFIK with the swivel-angle as free-var always finds a solution—as expected from Table 2—enabling smooth joint-trajectory.

and the Jacobian, which in turn was used to compute the manipulability ellipsoid. The solver then aimed to match a reference ellipsoid provided by a user demonstration (e.g., sweeping or pushing motions). We sampled 250 such configurations every 30 ms, akin to a lightweight model-predictive control loop.

As shown in Fig. 11 GeoFIK achieves lower computational times thanks to its screw-transformation design, where the Jacobian emerges naturally from the IK solution. Although HeLiu managed to complete the sweeping task, it proved slower in delivering joint–Jacobian pairs. IKFast again frequently produced no valid solutions (or an out-of-reach configuration), leading to task failure in the sweeping experiments, Figs. 12(b-c). GeoFIK, by contrast, consistently offered feasible joint trajectories while preserving the desired manipulability profile, underscoring the benefits of its geometry-aware method and multi-parameter redundancy resolution.

11 CONCLUSIONS

We introduced a fully geometric, screw-theory-based IK solver for the Franka Robot, accommodating multiple free parameters and automatically providing Jacobian information even faster than the joint configuration. By systematically capturing all geometrically valid solutions, our method, GeoFIK, overcomes the limitations of existing solvers that either fix only q_7 or neglect key geometric insights. Extensive quantitative benchmarks showed that our approach consistently outperforms baseline solvers in terms of reliability, completeness, and efficiency. Real-world experiments confirmed its resilience, enabling the robot to smoothly execute tasks and even when controlling less conventional variables, such as the swivel angle. We believe that the flexibility and robustness of GeoFIK can facilitate more advanced planning, control, and learning algorithms, thereby fulfilling the growing demand for speed and reliability in modern robotics.

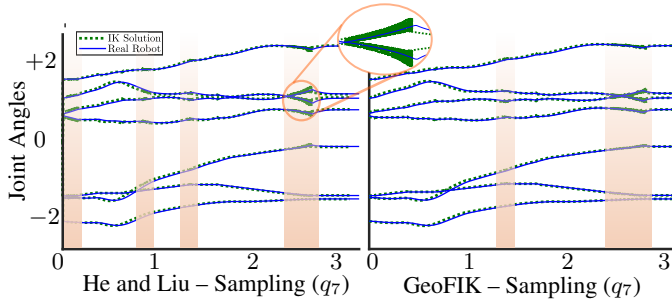


Figure 10: Trajectory tracking using IK solvers and sampling $q_7 \pm 10^\circ$. Sampling allows q_7 -locking IKs to complete the task, but the resulting trajectory includes chattering due to discontinuities (the overlapped green areas).

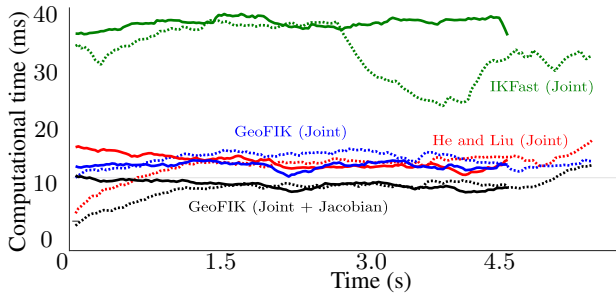


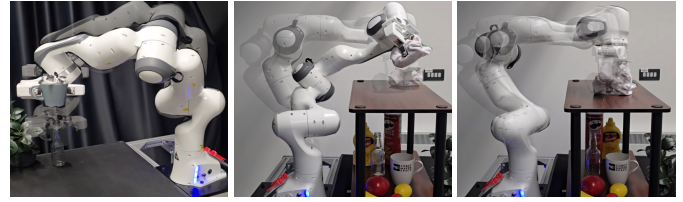
Figure 11: Computation time in tracking manipulability for sweeping (dashed) and pushing (solid) tasks.

ACKNOWLEDGEMENTS

This work is funded by StMWi Bayern (grant 5140951) and by the AIC.

REFERENCES

- [1] Franka Control Interface (FCI) - Panda description. https://frankaemika.github.io/docs/franka_ros.html#franka-description.
- [2] GeoFIK: Geometric IK solvers for the Franka Emika Panda arm. <https://github.com/PabloLopezCustodio/GeoFIK>. Accessed: 28-Feb-2025.
- [3] S. Chiaverini. Singularity-robust task-priority redundancy resolution for real-time kinematic control of robotic manipulators. *IEEE Trans. on Robotics and Automation*, 13(3):398–410, 1997.
- [4] P. Corke. Matlab Robotics Toolbox: Franka Emika Panda Kinematics & Singularities. <https://petercorke.com/robotics/franka-emika-panda-kinematics-and-singularities/>. Accessed: 29-08-24.
- [5] C. D. Crane III and J. Duffy. *Kinematic analysis of robot manipulators*. Cambridge university press, 1998.
- [6] R. Diankov. *Automated construction of robotic manipulation programs*. PhD thesis, Carnegie Mellon University, USA, 2010.
- [7] A. J. Elias and J. T. Wen. Redundancy parameterization and inverse kinematics of 7-DOF revolute manipulators. *Mechanism and Machine Theory*, 204:105824, 2024.



(a) IKFast EE Track (b) IKFast Sweep (c) GeoFIK Sweep

Figure 12: (a) IKFast traj. tracking, and (b)c IKFast and (c) GeoFIK sweeping tasks. IKFast often provides invalid solutions. In (a), the lack of solutions near the $\mathbf{q}(0)$ results in abrupt arm rotations exceeding torque reflexes. Similarly, in sweeping tasks, IKFast causes the arm to flip over lacking proper solutions. GeoFIK success in all tasks.

- [8] J. Elsner. Taming the panda with python: A powerful duo for seamless robotics programming and integration. *SoftwareX*, 24, 2023.
- [9] S. Feng, B. Burchfiel, and R. Tedrake. TRI’s Robots Learn New Manipulation Skills in an Afternoon. Here’s How. Medium (Toyota Research Institute), <https://medium.com/toyotaresearch/tris-robots-learn-new-skills-in-an-afternoon-here-s-how-2c30b1a8c573>. Accessed: 29-Aug-2024.
- [10] L. F. Figueredo, R. D. C. Aguiar, L. Chen, T. C. Richards, S. Chakrabarty, and M. Dogar. Planning to minimize the human muscular effort during forceful human-robot collaboration. *ACM Trans. on Human-Robot Interaction (THRI)*, 11(1):1–27, 2021.
- [11] Q. Gallouédec, N. Cazin, E. Dellandréa, and L. Chen. panda-gym: Open-Source Goal-Conditioned Environments for Robotic Learning. In *Proc. of the 4th Robot Learning Workshop: Self-Supervised and Lifelong Learning (NeurIPS)*, 2021.
- [12] C. R. Garrett, R. Chitnis, R. Holladay, B. Kim, T. Silver, L. P. Kaelbling, and T. Lozano-Pérez. Integrated task and motion planning. *Annual Review of Control, Robotics, and Autonomous Systems*, 4(Volume 4, 2021):265–293, 2021.
- [13] C. Gaz, M. Cagnetti, A. Oliva, P. Robuffo Giordano, and A. De Luca. Dynamic identification of the Franka Emika Panda Robot with retrieval of feasible parameters using penalty-based optimization. *IEEE Robotics and Automation Letters*, 4(4):4147–4154, 2019.
- [14] S. Haddadin. The franka emika robot: A standard platform in robotics research [survey]. *IEEE Robotics and Automation Magazine*, 31(4):136–148, 2024.
- [15] Y. He and S. Liu. Analytical inverse kinematics for Franka Emika panda—a geometrical solver for 7-DOF manipulators with unconventional design. In *IEEE Int. Conf. on Control, Mechatronics and Automation (ICCMA)*, 2021.
- [16] Y. He and S. Liu. Franka analytical IK. https://github.com/ffall007/franka_analytical_ik, 2024. Accessed: 28-Feb-2025.
- [17] R. Holladay, T. Lozano-Pérez, and A. Rodriguez. Force-and-motion constrained planning for tool use. In

- IEEE/RSJ International Conference on Intelligent Robots and Systems (IROS)*, pages 7409–7416, 2019.
- [18] L. Jiang, X. Huo, Y. Liu, and H. Liu. An integrated inverse kinematic approach for the 7-DOF humanoid arm with offset wrist. In *IEEE int. conf. on robotics & biomimetics (ROBIO)*, pages 2737–2742, 2013.
- [19] R. Kirschner, K. Karacan, A. Melone, et al. Categorizing robots by performance fitness into the tree of robots. *Nature Machine Intelligence*, 2025.
- [20] R. Laha, W. Wu, R. Sun, N. Mansfeld, L. F. Figueredo, and S. Haddadin. S*: On safe and time efficient robot motion planning. In *IEEE Int. Conf. on Robotics & Automation (ICRA)*, pages 12758–12764, 2023.
- [21] C. Lenz, M. Schwarz, A. Rochow, B. Pätzold, R. Memmesheimer, M. Schreiber, and S. Behnke. NimRo wins ANA Avatar XPRIZE Immersive Telepresence Competition: Human-Centric Evaluation and Lessons Learned. *International Journal of Social Robotics*, 2023. Published online Oct. 2023.
- [22] A. A. Oliva, F. Spindler, P. R. Giordano, and F. Chaumette. FrankaSim: A dynamic simulator for the Franka Emika robot with visual-servoing enabled capabilities. In *17th International Conference on Control, Automation, Robotics and Vision (ICARCV)*, pages 868–874, 2022.
- [23] M. Raghavan and B. Roth. Inverse kinematics of the general 6R manipulator and related linkages. *Journal of Mechanical Design*, 115(3):502–508, 09 1993.
- [24] D. Rakita, B. Mutlu, and M. Gleicher. Relaxedik: Real-time synthesis of accurate and feasible robot arm motion. In *Proceedings of Robotics: Science and Systems (RSS)*, 2018.
- [25] D. Rakita, H. Shi, B. Mutlu, and M. Gleicher. Collisionik: A per-instant pose optimization method for generating robot motions with environment collision avoidance. In *IEEE International Conf. on Robotics and Automation (ICRA)*, pages 9995–10001, 2021.
- [26] J. M. Selig. *Geometric fundamentals of robotics*. Springer Science & Business Media, 2007.
- [27] B. Siciliano, L. Sciavicco, L. Villani, and G. Oriolo. *Robotics: Modelling, Planning and Control*. Springer Publishing Company, Incorporated, 2010.
- [28] S. Tittel. Analytical solution for the inverse kinematics problem of the Franka Emika panda seven-DOF lightweight robot arm. In *20th Intern. Conference on Advanced Robotics (ICAR)*, pages 1042–1047, 2021.
- [29] M. Tröbinger, A. Naceri, X. Chen, H. Sadeghian, and S. Haddadin. Identification of a generalized base inertial parameter set of robotic manipulators considering mounting configurations. In *2023 IEEE International Conference on Robotics and Automation (ICRA)*, pages 11502–11508, 2023.
- [30] Y. Wang, L. Li, and G. Li. An analytical solution for inverse kinematics of 7-DOF redundant manipulators with offsets at elbow and wrist. In *2022 IEEE 6th Information Technology and Mechatronics Engineering Conference (ITOEC)*, volume 6, pages 1096–1103. IEEE, 2022.
- [31] X. Yang, Z. Zhao, Z. Xu, Y. Li, J. Zhao, and H. Liu. General inverse kinematics method for 7-DOF offset manipulators based on arm angle parameterization. *Acta Astronautica*, 202:263–277, 2023.